Accelerated Publications

Branched Activation- and Catalysis-Specific Pathways for Electron Relay to the Manganese/Iron Cofactor in Ribonucleotide Reductase from *Chlamydia trachomatis*[†]

Wei Jiang,[‡,§] Lana Saleh,[‡,§,||] Eric W. Barr,[‡] Jiajia Xie,[‡] Monique Maslak Gardner,[‡] Carsten Krebs,*[,‡,⊥] and J. Martin Bollinger, Jr.*[,‡,⊥]

Department of Biochemistry and Molecular Biology and Department of Chemistry, The Pennsylvania State University, University Park, Pennsylvania 16802

Received May 12, 2008; Revised Manuscript Received June 27, 2008

ABSTRACT: A conventional class I (subclass a or b) ribonucleotide reductase (RNR) employs a tyrosyl radical (Y•) in its R2 subunit for reversible generation of a 3′-hydrogen-abstracting cysteine radical in its R1 subunit by proton-coupled electron transfer (PCET) through a network of aromatic amino acids spanning the two subunits. The class Ic RNR from the human pathogen *Chlamydia trachomatis* (*Ct*) uses a Mn^{IV}/Fe^{III} cofactor (specifically, the Mn^{IV} ion) in place of the Y• for radical initiation. *Ct* R2 is activated when its Mn^{II}/Fe^{II} form reacts with O_2 to generate a Mn^{IV}/Fe^{IV} intermediate, which decays by reduction of the Fe^{IV} site to the active Mn^{IV}/Fe^{III} state. Here we show that the reduction step in this sequence is mediated by residue Y222. Substitution of Y222 with F retards the intrinsic decay of the Mn^{IV}/Fe^{IV} intermediate by ∼10-fold and diminishes the ability of ascorbate to accelerate the decay by ∼65-fold but has no detectable effect on the catalytic activity of the Mn^{IV}/Fe^{III}−R2 product. By contrast, substitution of Y338, the cognate of the subunit interfacial R2 residue in the R1 ⇔ R2 PCET pathway of the conventional class I RNRs [Y356 in *Escherichia coli* (*Ec*) R2], has almost no effect on decay of the Mn^{IV}/Fe^{IV} intermediate but abolishes catalytic activity. Substitution of W51, the *Ct* R2 cognate of the cofactor-proximal R1 ⇔ R2 PCET pathway residue in the conventional class I RNRs (W48 in *Ec* R2), both retards reduction of the Mn^{IV}/Fe^{IV} intermediate and abolishes catalytic activity. These observations imply that *Ct* R2 has evolved branched pathways for electron relay to the cofactor during activation and catalysis. Other R2s predicted also to employ the Mn/Fe cofactor have Y or W (also competent for electron relay) aligning with Y222 of *Ct* R2. By contrast, many R2s known or expected to use the conventional Y•-based system have redox-inactive L or F residues at this position. Thus, the presence of branched activation- and catalysis-specific electron relay pathways may be functionally important uniquely in the Mn/Fe-dependent class Ic R2s.

Ribonucleotide reductases (RNRs)[1] catalyze the reduction of ribonucleotides to deoxyribonucleotides, the precursors for DNA synthesis and repair (*1*). This remarkable reaction proceeds via a free radical mechanism. Conventional class I RNRs [e.g., from *Homo sapiens* or aerobically growing *Escherichia coli* (*Ec*)] consist of R1 and R2 subunits. R1 is the catalytic subunit and contains the site of ribonucleotide reduction. R2 is the cofactor subunit, harboring a stable tyrosyl radical (Y•) in the proximity of a carboxylate-bridged $Fe_2^{III/III}$ cluster (*2*). It is believed that, during catalysis, the Y• in R2 transiently oxidizes a conserved cysteine residue in the R1 active site to a cysteinyl radical (C•) (*3*) by a long-distance (∼35 Å), intersubunit (*4*), proton-coupled electron transfer (PCET) reaction (*5*). The C• then initiates reduction of the substrate by abstracting its 3′-hydrogen atom (*3, 6–9*). For the best-studied class I RNR from *Ec*, it is thought that the PCET step is mediated by several redox-active amino acid residues, including W48 and Y356 in R2 and Y730 and Y731 in R1 (*3–5, 10–17*).

The cofactor in R2 is generated in a post-translational autoactivation reaction, in which O_2 adds to the reduced ($Fe_2^{II/II}$) diiron cluster (*18, 19*). In this reaction, O_2 is reduced by four electrons to the oxidation state of water. The reduction is balanced by oxidation of two Fe^{II} ions to Fe^{III},

[†] This work was supported by the National Institutes of Health (Grant GM-55365 to J.M.B.), the Beckman Foundation (Young Investigator Award to C.K.), and the Dreyfus Foundation (Teacher Scholar Award to C.K.).

* To whom correspondence should be addressed. J.M.B.: Department of Chemistry, 336 Chemistry Building, University Park, PA 16802. Phone: (814) 863-5707. Fax: (814) 865-2927. E-mail: jmb21@psu.edu. C.K.: Department of Chemistry, 332 Chemistry Building, University Park, PA 16802. Phone: (814) 865-6089. Fax: (814) 865-2927. E-mail: ckrebs@psu.edu.

[‡] Department of Biochemistry and Molecular Biology.

[§] L.S. and W.J. both made contributions warranting primary authorship. Prior to the recognition of the enzyme's manganese requirement, L.S. discovered the electron relay function of Y222 in the reaction of the inactive diiron form. W.J. carried out all experiments proving that the residue functions also during activation of the Mn/Fe form.

[||] Present address: New England Biolabs, 240 County Rd., Ipswich, MA 01938.

[⊥] Department of Chemistry.

[1] Abbreviations: RNR, ribonucleotide reductase; *Ec*, *Escherichia coli*; Y•, tyrosyl radical; C•, cysteinyl radical; *Ct*, *Chlamydia trachomatis*; EPR, electron paramagnetic resonance; PCET, proton-coupled electron transfer; CDP, cytidine 5′-diphosphate; dCDP, 2′-deoxycytidine 5′-diphosphate; wt, wild-type; DTT, dithiothreitol; EDTA, ethylenediaminetetraacetic acid.

10.1021/bi800881m CCC: $40.75
Published on Web 07/26/2008

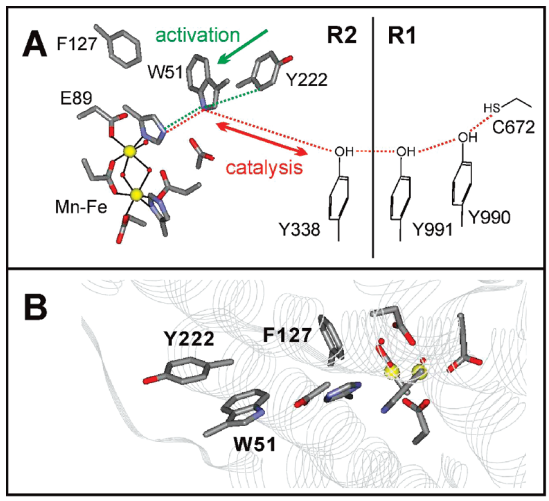

FIGURE 1: Branched electron relay pathways in *Ct* RNR. (A) The catalysis-specific intersubunit pathway between the Mn/Fe cluster in R2 and the conserved cysteine residue in R1, C672, is indicated by the red dotted lines. The conserved residues proposed to participate in electron relay are indicated. The activation-specific pathway is indicated by green dotted lines. This figure was adapted from the docking model for *Ec* RNR (*4, 5*). (B) Schematic based on the X-ray crystal structure of *Ct* R2 (*42*) showing the positions of residues in the aforementioned electron relay pathways.

oxidation of Y122 by one electron to the radical, and transfer of an "extra" electron (*20–22*). During activation of *Ec* R2, the extra electron is transferred to a very reactive adduct between the $Fe_2^{II/II}$ cluster and O_2 by oxidation of the near-surface PCET pathway residue, W48 (*23–25*). The resulting state contains an $Fe_2^{III/IV}$ intermediate, **X** (*19, 26–31*), and a W48 cation radical ($W48^{+\bullet}$) (*23, 24*), which is reduced in vitro by exogenous reductants (e.g., Fe^{II} or ascorbate) (*23*). Intermediate **X** oxidizes the nearby tyrosine residue (Y122) in the final and slowest step of the reaction, yielding the active $Fe_2^{III/III}/Y^{\bullet}$ form of the protein (*19, 20*). When the activation reaction is carried out in the presence of >10 mM Mg^{2+}, $W48^{+\bullet}$ engages in a rapid redox equilibrium with Y356 (*32*), the next R2 residue in the proposed R1 ⟺ R2 PCET pathway (*4, 13, 33*). The reversible formation of the $Y356^{\bullet}$ radical initiates an efficient pathway for decay of $W48^{+\bullet}$ even in the absence of a facile one-electron reductant (*32*). Thus, *Ec* R2 utilizes the same two-residue pathway for electron relay to its cofactor during both activation and catalysis.

We recently showed that the class Ic RNR from *Chlamydia trachomatis* (*Ct*) employs a high-valent, heterobinuclear Mn^{IV}/Fe^{III} cofactor in place of the $Fe_2^{III/III}/Y^{\bullet}$ cofactor of the conventional class I system (*34, 35*). Use of a mechanism-based inactivator (2′-deoxy-2′-azidoadenosine-5′-diphosphate) provided evidence that the Mn^{IV}/Fe^{III} cofactor undergoes reduction to Mn^{III}/Fe^{III} during catalysis (*34*). Results obtained upon treatment of the enzyme with the well-known class I RNR inhibitor, hydroxyurea, provided additional support for this hypothesis (*36*). Presumably, reduction of the Mn^{IV} ion of the cofactor to Mn^{III} generates the $C^{\bullet}$ in the *Ct* R1 subunit via the intersubunit PCET pathway, of which all residues are conserved (Figure 1A, red dotted lines) (*37*). In analogy to the conventional ($Fe_2^{III/III}/Y^{\bullet}$) R2 proteins, activation of *Ct* R2 entails reaction of its fully reduced (Mn^{II}/Fe^{II}) cluster with O_2 (*34*). A Mn^{IV}/Fe^{IV} intermediate accumulates almost stoichiometrically and then decays by slow reduction of the Fe^{IV} site to Fe^{III} (*38*). This decay step is analogous to the relay of the extra electron to the diiron site by W48 during activation of *Ec* R2 (*23*). However, no evidence of accumulation of $W^{+\bullet}$ from the corresponding *Ct* R2 residue, W51, was obtained (*38*).

In this study, we show that Y222, a surface residue aligning with the redox-inactive L233 of *Ec* R2, cooperates with W51 to relay the extra electron to the Mn^{IV}/Fe^{IV} intermediate during activation of *Ct* R2 (Figure 1A, green dotted lines). The irrelevance of Y222 and the importance of Y338 (the cognate of *Ec* Y356) for catalytic activity imply that, unlike the *Ec* protein, *Ct* R2 uses distinct electron-relay pathways for activation and catalysis (Figure 1A, red dotted lines). The strict conservation of an ET-competent residue (Y or W) at the position corresponding to Y222 in other presumptively Mn/Fe-dependent R2 proteins[2] suggests that the novel, activation-specific, electron relay element is functionally important in the class Ic RNRs.

MATERIALS AND METHODS

Construction of Vectors for Overexpressing His_6-Affinity-Tagged Versions of Ct R2 Variants Y222F, Y338F, and W51F. Construction of the plasmid vector, pET28a-*Ct*R2-wt, which directs overexpression of the N-terminally His_6-tagged wild-type (wt) *Ct* R2 protein, was described previously (*34*). The vector for directing overexpression of the Y222F variant was constructed by using the Quikchange XL site-directed mutagenesis kit (Stratagene, La Jolla, CA), with pET28a-*Ct*R2-wt as the template and primers 1 (5′-GGA GAA CAA TAT CAA TTC AT**C TTA AG**A GAT GAG ACA ATC C-3′; *Afl*II site in bold) and 2 (5′-GGA TTG TCT CAT CT**C TTA AG**A TGA ATT GAT ATT GTT CTC CAA TAC C-3′; *Afl*II site in bold) encoding the desired substitution (underlined in primer sequences). The Quikchange kit was also used to construct the vector for the W51F variant, with the same template and primers 3 (5′-GGC TGC GCA AAT AAC TTT CTC CCT ACA GAG ATC C**CC ATG G**GG AAA GAC ATC G-3′; *Nco*I site in bold) and 4 (5′-CTT TCC **CCA TGG** GGA TCT CTG TAG GGA GAA AGT TAT TTG CGC AGC C-3′; *Nco*I site in bold) introducing the desired substitution (underlined). The sequences of the coding regions of both vectors were verified by ACGT, Inc. (Wheeling, IL).

The Y338F substitution was introduced by the polymerase chain reaction (PCR) by using pET28a-*Ct*R2-wt as the template and primers 5 (5′-TTA ACG GTT **CAT ATG** CAA GCA GAT ATT TTA GAT GG-3′; *Nde*I restriction site in bold) and 6 (5′-GGT GGT G**CT CGA G**CT ACC AAG TTA AGC TTG CTG CAT GTT GAA ATT CTA TAA CCC-3′; *Xho*I site in bold) to introduce the desired substitution (underlined). The 1086 bp PCR fragment was gel purified, restricted with *Nde*I and *Xho*I, repurified, and ligated with *Nde*I- and *Xho*I-restricted pET28a-*Ct*R2-wt. The sequence of the coding region of the vector was verified.

[2] Presumptive Mn/Fe-dependent R2 proteins were identified by pBLAST queries of the NCBI nr protein database with the sequence of *Ct* R2. As previously reported (*42*), R2s with F and E aligning with F127 and E89 of *Ct* R2 (which are Y122 and D84, respectively, in *Ec* R2) are assigned to class Ic and are expected to employ Mn^{IV}/Fe^{III} cofactors. Among the ~30 presumptive Mn/Fe-dependent class Ic R2s identified by this search, all possess Y or W at the position aligning with Y222 of *Ct* R2.

Overexpression and Purification of Ct R2 Proteins. The variant *Ct* R2 proteins were prepared as previously described for the wt protein (*34*). His_6-tagged proteins were overexpressed in *E. coli* BL21(DE3) (Novagen, Madison, WI), purified by metal ion affinity chromatography, and depleted of metal ions by the previously described reductive chelation and EDTA dialysis steps (*34*). The concentrations of apoproteins were determined by absorbance at 280 nm with monomeric molar absorptivities (57750 M^{-1} cm^{-1} for the wt, 56470 M^{-1} cm^{-1} for Y222F and Y338F, and 52060 M^{-1} cm^{-1} for W51F) calculated by the method of Gill and von Hippel (*39*).

Mössbauer-Spectroscopic Characterization of the Mn^{IV}/Fe^{III} Complexes of the Ct R2 Proteins. The Mn^{IV}/Fe^{III} products of the O_2 reactions of wt, Y222F, Y338F, and W51F *Ct* R2 proteins were prepared with ~95% ^{57}Fe-enriched Fe^{II} as previously described (*40*). The Mössbauer spectrometer has been described previously (*41*).

Stopped-Flow Absorption and Freeze-Quench EPR Kinetics Experiments. The stopped-flow and freeze-quench apparatus and procedures and the EPR spectrometer have been described previously (*41*). Kinetic traces from the reactions of the Mn^{II}/Fe^{II}−R2 complexes with O_2 were analyzed by nonlinear regression according to eq 1, which gives absorbance as a function of time (A_t) for a system of two parallel, irreversible, first-order reactions in terms of rate constants for the two steps (k_1 and k_2), their associated amplitudes (ΔA_1 and ΔA_2), and the absorbance at time zero (A_0).

$$A_t = A_0 + \Delta A_1[1 - \exp(-k_1 t)] + \Delta A_2[1 - \exp(-k_2 t)] \quad (1)$$

Although the *Ct* R2 reaction comprises two sequential irreversible steps, formation of the intermediate is so much faster than its decay ($k_1 > 300k_2$) that the equation describing the sequential case simplifies to that describing the parallel case. (The approximation of the second-order formation step as a pseudo-first-order step is acceptable with the excess of O_2 employed.) The kinetics of the Mn^{IV}/Fe^{IV}−R2 intermediate predicted by the fit rate constants were calculated according to eq 2, to which eq 1 simplifies in considering concentration rather than absorbance (again, appropriate only for the case of $k_1 \gg k_2$).

$$[Mn^{IV}/Fe^{IV}-R2]_t = [Mn^{II}/Fe^{II}-R2]_0[\exp(-k_2 t) - \exp(-k_1 t)] \quad (2)$$

Determination of Catalytic Activities of the Ct R2 Proteins. The same Mn^{IV}/Fe^{III}−R2 samples characterized by Mössbauer spectroscopy were used to determine the catalytic activities of the wt and variant proteins. Activity was quantified by the previously described mass spectrometric assay (*34*). In assays of the active wt and Y222F R2 proteins, 1 μM R2 monomer was used. To improve the detection limit in assays of the inactive Y338F and W51F variant proteins, 40 μM R2 monomer was used. Reactions were initiated by addition of R2. They contained in a final volume of 200 μL a 10-fold excess of Δ(1−248) *Ct* R1 (*34, 37*), 2 mM CDP, 0.5 mM ATP, and 10 mM DTT in 20 mM Na-Hepes buffer (pH 7.6). They were allowed to proceed at 37 °C for 30 min. They were terminated by addition of HCl to a final concentration of 100 mM. Precipitated protein was removed by filtration through a Microcon YM-3 device (Millipore Corp.). A 10 μL aliquot of the filtrate was injected with a mobile phase of 10% acetonitrile, 90% water, and 0.5 mM HCl running at 0.05 mL/min onto a Waters (Milford, MA) Micromass ZQ 2000 mass spectrometer with an electrospray ionization probe operating in the negative ion mode. Spectrometer conditions were as follows: capillary voltage, 4.00 kV; cone voltage, −50 V; extractor voltage, −2 V; RF lens voltage, 0 V; source temperature, 80 °C; desolvation temperature, 450 °C; desolvation gas flow rate, 150 L/h; cone gas flow rate, 60 L/h. The ion currents at *m*/*z* 402 and 386 (M^- for CDP and dCDP, respectively) were continuously and simultaneously monitored after injection. Triplicate injections of each reaction sample were performed. The ratio of the heights of the CDP and dCDP peaks to the sum of these peak heights was multiplied by the initial concentration of CDP (2 mM) to give the concentrations of substrate and product in each reaction sample. Validation of the assay method is provided in the Supporting Information.

RESULTS

Discovery of Electron Relay by Y222 during O_2 Activation by the $Fe_2^{II/II}$ Form of Ct R2. Prior to our discovery that the active form of *Ct* R2 contains a heterobinuclear Mn^{IV}/Fe^{III} cofactor that forms by reaction of the Mn^{II}/Fe^{II} cluster with O_2 (*34*), our initial experiments on the catalytically inactive homobinuclear (Fe_2) form of the protein revealed the participation of Y222 in electron relay to the cofactor during O_2 activation. Reaction of the $Fe_2^{II/II}$−R2 protein (1.5 equiv of Fe^{II} per monomer) at 5 °C with O_2 results in rapid development of the sharp ~410 nm absorption signature of a tyrosyl radical (Figure 2A, marked by the arrow). This peak decays within 50 s to yield the featureless spectrum of the $Fe_2^{III/III}$ product (blue spectrum).[3] During activation of *Ec* R2, a transient W48 cation radical ($W48^{+\bullet}$) accumulates under these conditions (*23, 24*), and the presence of a high concentration (>10 mM) of Mg^{2+} engages a rapid redox equilibrium between W48 and the next residue in the PCET pathway, Y356, resulting in co-accumulation of $Y356^\bullet$ and $W48^{+\bullet}$ (*32*). To test whether the transient $Y^\bullet$ detected in the *Ct* R2 reaction resides on Y338, the cognate of *Ec* R2 residue Y356, Y338 was replaced with F and O_2 activation by the Y338F variant examined. The absorption signature of the transient $Y^\bullet$ is not diminished in the variant (Figure 2B, arrow) and is even somewhat enhanced, implying that Y338 is not the primary site of the transient $Y^\bullet$ in the *Ct* R2 reaction. Similarly, substitution (by F) of Y112, a residue near the cofactor but with no cognate in the *Ec* protein and no known or suspected role in PCET, does not diminish the absorption signature of the transient $Y^\bullet$ (not shown).

Prospecting for other candidates for the site of the transient $Y^\bullet$, we noted that Y222 is close to W51 (see Figure 1 (*42*)), the *Ct* R2 cognate of W48 in *Ec* R2, and hypothesized that it could be the site of the transient $Y^\bullet$. Indeed, the signature of the transient $Y^\bullet$ is not observed (or is much less prominent) in the reaction of the Y222F variant of *Ct* R2 (Figure 2C). Rather, a new, broad, transient absorption centered at ~550 nm develops instead (marked by the arrow). This feature is

[3] The lack of intense absorption features for the $Fe_2^{III/III}$ cluster in the 360−600 nm regime, which contrasts with the spectrum of the $Fe_2^{III/III}$ cluster in *Ec* R2, is consistent with the conclusion from X-ray crystallography that the *Ct* R2 product has two bridging hydroxo or water ligands (*42*) rather than the single μ-oxo of the *Ec* cluster (*12*).

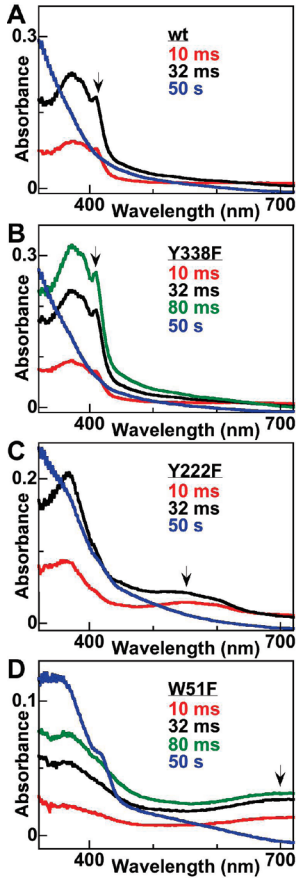

FIGURE 2: Time-dependent UV−visible absorption spectra from the reactions of the $Fe_2^{II/II}$ forms of (A) wt *Ct* R2 and its (B) Y338F, (C) Y222F, and (D) W51F variants with O_2 at 5 °C. Spectra were recorded at the indicated reaction time after mixing of an O_2-free solution of 0.20 mM R2 (0.40 mM monomer) and 0.60 mM Fe^{II} with an equal volume of O_2-saturated buffer. For each spectrum that is shown, the 1.3 ms spectrum has been subtracted from the experimental spectrum at the indicated reaction time to illustrate the changes with time.

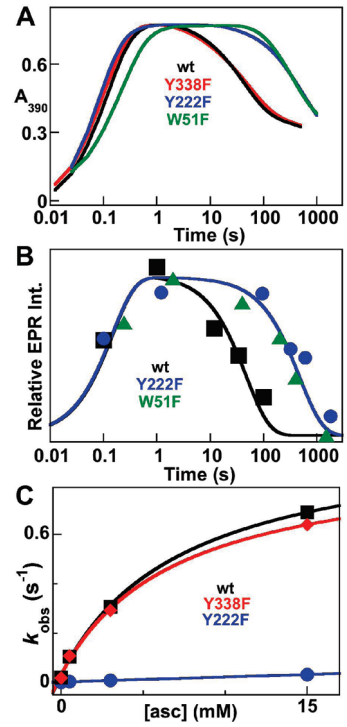

FIGURE 3: Kinetics of the Mn^{IV}/Fe^{IV} intermediate during reaction of the Mn^{II}/Fe^{II} complexes of wt (black), Y338F (red), Y222F (blue), and W51F (green) R2 proteins at 5 °C with O_2, and the effect of ascorbate thereupon. (A) Absorbance vs time traces for the reactions in the absence of ascorbate. The reactions were initiated by mixing of an O_2-free solution of 0.40 mM R2 (0.80 mM R2 monomer), 0.32 mM Fe^{II}, and 0.96 mM Mn^{II} with an equal volume of O_2-saturated buffer at 5 °C. (B) Kinetics of the Mn^{IV}/Fe^{IV} intermediate from the intensity of its six-line EPR spectrum centered at $g \sim 2$. The freeze-quench EPR samples were prepared under reaction conditions identical to those described for panel A. The solid lines are kinetics of the intermediate for the wt (black) and Y222F (blue) reactions calculated according to rate constants extracted from the stopped-flow results: $k_{form,wt} = 6.7\ s^{-1}$, $k_{decay,wt} = 0.021\ s^{-1}$, $k_{form,Y222F} = 7.0\ s^{-1}$, and $k_{decay,Y222F} = 0.0021\ s^{-1}$. Spectrometer conditions were as follows: temperature, 14.0 ± 0.2 K; microwave frequency, 9.45 GHz; microwave power, 20 μW; modulation frequency, 100 kHz; modulation amplitude, 10 G; scan time, 167 s; and time constant, 167 ms. (C) Dependence of the apparent first-order rate constant for decay of the Mn^{IV}/Fe^{IV} intermediate (monitored by absorbance at 390 nm) on the concentration of ascorbate. The stopped-flow experiments were carried out under conditions identical to those described for panel A, with the exception of the presence of ascorbate (sufficient to give the indicated concentrations after mixing) in the protein solution. The rate constants for decay of the Mn^{IV}/Fe^{IV} intermediate were extracted by fitting eq 1 to the 390 nm kinetic traces (Figure S3).

reminiscent of the signature of $W48^{+\bullet}$ in the *Ec* R2 reaction (*23, 24*). These observations suggest that Y222 is the site of the transient $Y^{\bullet}$ in the reaction of the wild-type *Ct* R2 protein and that its substitution with F causes accumulation of $W^{+\bullet}$, presumably residing on W51. The latter assignment is supported by experiments with the W51F variant (Figure 2D). Reaction of the $Fe_2^{II/II}$ complex of W51F *Ct* R2 with O_2 does not result in accumulation of the transient absorption band at ~550 nm. Rather, yet another transient absorption feature, a broad intense band at ~700 nm (arrow) that our previous work on D84E variants of *Ec* R2 implies can be attributed to a μ-(1,2-peroxo)−$Fe_2^{III/III}$ complex (*43–45*), is observed.[4] Thus, an oxidized diiron intermediate accumulates in place of $Y222^{\bullet}$ (or $W51^{+\bullet}$) in the W51F variant. The simplest interpretation of these results is that W51 and Y222 cooperate to relay an electron to the diiron cluster during O_2 activation, with $Y222^{\bullet}$ being the more stable of the pathway radicals.

Evidence for Electron Relay by Y222 Also during O_2 Activation by the Mn^{II}/Fe^{II} Form of Ct R2. To test whether the novel electron relay element, Y222, functions during formation of the active Mn^{IV}/Fe^{III} form of *Ct* R2, the kinetics of the O_2 reactions of the aforementioned variant proteins (W51F, Y222F, and Y338F) in their Mn^{II}/Fe^{II} forms were compared to those of the wt protein (Figure 3A).[5] The substitutions have either no effect (Y222F and Y338F) or a minor effect (W51F) on the development of the 390 nm

[4] The Mössbauer spectra of freeze-quenched samples exhibit the signature of the peroxide complex (*43, 46*) and confirm this assignment. These results will be presented elsewhere.

[5] As previously observed for the $Fe_2^{IV/IV}$ complex, **Q**, in the reaction of soluble methane monooxygenase (*47*), the Mn^{IV}/Fe^{IV} intermediate in *Ct* R2 is photosensitive: its decay is accelerated by the intense white light source used with the photodiode array detector in our previous studies. The kinetic traces shown in Figure 3A were acquired with monochromatic 390 nm light and a photomultiplier detector. Figure S1 illustrates the marked acceleration of decay of the intermediate by the white light source in the reaction of R2 Y222F.

absorption of the Mn^{IV}/Fe^{IV} intermediate, and the Y338F substitution has no effect on the decay of this feature. By contrast, both the W51F and the Y222F substitutions retard decay of this feature by ~10-fold (Table 1). Freeze-quench EPR experiments on the reactions of the wt, W51F, and Y222F were conducted to confirm that the absorbance-versus-time traces accurately reflect the kinetics of the intermediate (Figure 3B). The kinetics (black squares, blue circles, and green triangles) extracted from the intensities of the sharp six-line EPR feature of the Mn^{IV}/Fe^{IV} complex (Supporting Information, Figure S2) agree well with traces calculated by using the rate constants extracted from the stopped-flow data (solid black and blue lines), confirming that both the W51F and Y222F mutations stabilize the intermediate by retarding its reduction.

It was previously shown that ascorbate can accelerate the reduction of the Mn^{IV}/Fe^{IV} intermediate in the reaction of wt *Ct* R2 (*38*). Additional stopped-flow absorption experiments were conducted to test whether reduction by ascorbate is mediated by Y222 (Figure 3C). As previously reported, decay of the intermediate is accelerated with a hyperbolic dependence on ascorbate concentration in the reaction of the wt protein (black squares and fit line). The Y338F substitution has no significant effect on this behavior (red diamonds and fit line), consistent with its failure to retard the intrinsic (i.e., in the absence of ascorbate) decay of the intermediate. By contrast, the Y222F substitution drastically diminishes (by ~65-fold) the efficiency of ascorbate reduction (blue circles and fit line) from an apparent second-order rate constant (k) of $(1.3 \pm 0.3) \times 10^{-1}$ mM^{-1} s^{-1} for the wt and Y338F proteins to a k of $(2.0 \pm 0.5) \times 10^{-3}$ mM^{-1} s^{-1} for the Y222F variant (Table 1). The results imply that Y222 mediates reduction of the intermediate both in the absence and in the presence of ascorbate.

Verification by Mössbauer Spectroscopy of Formation of the Mn^{IV}/Fe^{III} Product in the Reactions of the Variant R2s. To verify that, despite the altered kinetics, decay of the Mn^{IV}/Fe^{IV} intermediate in the W51F and Y222F variants still yields the Mn^{IV}/Fe^{III} product previously described for the wt protein, Mössbauer spectra of the products were recorded (Figure 4). The Mn^{IV}/Fe^{III} cofactor has a triplet ($S_{total} = 1$) ground state resulting from antiferromagnetic coupling of its Mn^{IV} ($S_{Mn} = {}^3/_2$) and high-spin Fe^{III} ($S_{Fe} = {}^5/_2$) ions. It gives rise to a sharp quadrupole doublet at 4.2 K in zero field and a diagnostic broadening (due to the hyperfine interaction between the $S = 1$ electron spin ground state and the ^{57}Fe nuclear spin) in the presence of weak external magnetic fields (*35*). Products of the Y222F, Y338F, and W51F reactions have spectra essentially identical to those of the wt protein in both 0 and 53 mT field, implying that all reactions form the Mn^{IV}/Fe^{III} cofactor.[6]

Catalytic Activities of wt and Variant Ct R2s Implying Branched Activation- and Catalysis-Specific Electron Relay Pathways. The capacities of the wt and variant R2 products characterized by Mössbauer spectroscopy to support RNR activity in the presence of *Ct* R1 were quantified to examine the roles of the three aromatic residues in catalysis. The wt and Y222F *Ct* R2 samples supported indistinguishable activities of 0.60 ± 0.06 and 0.58 ± 0.02 s^{-1} (mean ± standard deviation of four trials), respectively, implying that Y222 has no important role in the intersubunit PCET step that initiates turnover. By contrast, the activities of the Y338F and W51F variants were less than the detection limit of the assay (0.001 s^{-1}; Table 1), suggesting that Y338 and W51, like their cognates in the mouse and *Ec* R2 proteins (*13, 14, 33*), are both essential for the intersubunit PCET step. Thus, *Ct* R2 uses branched electron relay pathways for activation (W51−Y222) and catalysis (W51−Y338), of which the former is absent in *Ec* R2.

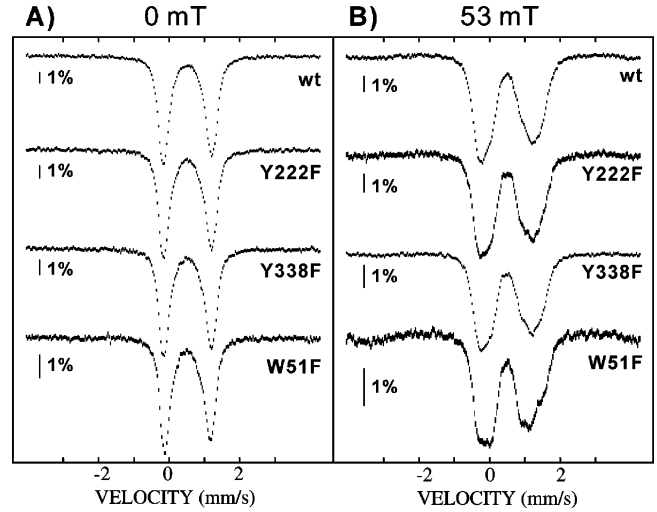

FIGURE 4: Mössbauer spectra of the final products of the O_2 reactions of the Mn^{II}/Fe^{II} cluster in wt, Y222F, Y338F, and W51F *Ct* R2. Spectra were collected at 4.2 K in external magnetic fields of 0 (A) and 53 mT (B) oriented parallel to the γ-beam. Samples were prepared as previously described (*40*) and concentrated to ~3 mM monomer prior to being frozen in liquid nitrogen. Spectra recorded over a wider range of Doppler velocities are shown in Figure S4.

DISCUSSION

Previous studies on the activation of the conventional $Fe_2^{III/III}/Y^{\bullet}$-dependent *Ec* and *Mus musculus* (mouse) R2 proteins have extensively documented the requirement for, and mechanism of, the transfer of the extra electron that balances the four-electron reduction of O_2 with the oxidation of two Fe^{II} ions and the tyrosine residue by one electron each (*19–23, 25, 32, 48*). The same requirement applies to activation of the Mn/Fe-dependent *Ct* R2 (*34*), but comparison of published data for this reaction (*38*) with those for the conventional R2 proteins suggests that kinetic details of the steps are quite different. It has been shown that diiron−O_2 complexes that are more oxidized than the product ($Fe_2^{III/III}$) cluster by two electrons (i.e., peroxo−$Fe_2^{III/III}$ or $Fe_2^{IV/IV}$ complexes) are fleeting during activation of the conventional R2 proteins (*23, 49*), at least in part because transfer of the extra electron from the cofactor-proximal PCET tryptophan residue (W48 in *Ec* R2) is so rapid (>400 s^{-1} at 5 °C in the *Ec* R2 reaction) (*23*). Further evidence suggests that this electron relay step occurs concomitantly (perhaps even concertedly) with cleavage of the O−O bond of a (putatively) peroxo−$Fe_2^{III/III}$ complex (*50*). The coupling of the oxidation of the tryptophan to O−O bond cleavage should make this

[6] The 53 mT spectra display some broad absorption at −4 and +4 mm/s. Spectra collected over a wider range of Doppler velocities (Figure S4) reveal that these features are caused by a paramagnetic complex. The spectra resemble those previously reported for the Mn^{III}/Fe^{III} complex ($S_{total} = {}^1/_2$) (*40*).

Scheme 1: Comparison of the Kinetic Mechanisms of Electron Relay to the Dimetal Center of *Ct* R2 during O_2 Activation by the $Fe_2^{II/II}$ (top) and Mn^{II}/Fe^{II} (bottom) Forms of the Protein

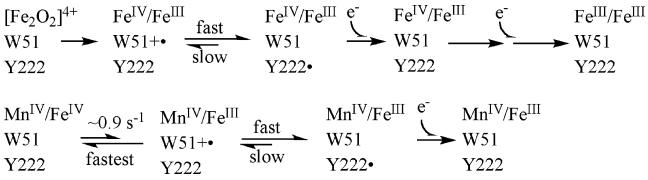

step thermodynamically favorable, resulting in the observed accumulation of the amino acid radical ($W^{+\bullet}$) (*23, 24*). By contrast, previous work on activation of *Ct* R2 revealed stoichiometric accumulation of the Mn^{IV}/Fe^{IV} complex, in which the O−O bond of O_2 has presumably already been cleaved (without net reduction), and no evidence for the accumulation of an amino acid radical during the subsequent, very slow reduction of the Mn^{IV}/Fe^{IV} complex to the stable, catalytically active Mn^{IV}/Fe^{III} form (*38*). In this case, the failure of a state containing the Mn^{IV}/Fe^{III} cofactor and an amino acid radical [the cognate of the $\mathbf{X}-W48^{+\bullet}$ "diradical" state in *Ec* R2 (*23*)] to accumulate could be explained by the lack of coupling of amino acid oxidation to O−O cleavage and the relatively modest reduction potential of the Mn^{IV}/Fe^{IV} intermediate (Scheme 1, bottom). It appears that substitution of the metal ion is more important than active site tuning in causing these differences, given that addition of O_2 to the $Fe_2^{II/II}$ cluster in *Ct* R2 *does* result (as in the *Ec* reaction) in the rapid accumulation of a state containing the $Fe_2^{III/IV}$ complex, **X** [shown previously (*42, 51–53*)], and an amino acid radical (Figure 2A,B and Scheme 1, top). The difference in the location of the transient radical in the diiron reactions (Y222 in *Ct* R2 vs W48 in *Ec* R2) can be explained by the lower reduction potential of (neutral) $Y^{\bullet}$ compared to $W^{+\bullet}$ (*5*). The phenolic hydroxyl of Y222 projects outward from the surface of *Ct* R2 into solution (Figure 1B) and should readily lose its proton to solvent or buffer upon phenol oxidation, localizing the "hole" at this site in preference to the more solvent-protected W51, which hydrogen bonds via its indole NH group to Asp226 (*42*) and may lose its proton less readily upon oxidation to the cation radical. From a chemical perspective, these considerations can explain the importance of the additional electron relay element in the Mn/Fe-dependent R2: the more favorable oxidation of Y222 (by PCET) may be required for efficient electron relay to the relatively stable Mn^{IV}/Fe^{IV} complex.

The biological and evolutionary rationale for the additional electron relay element is less apparent. The Y222F variant successfully assembles the Mn^{IV}/Fe^{III} cofactor and is then fully catalytically active. Thus, in vitro and upon a single activation event, Y222 is completely dispensable. The conservation among all presumptively Mn/Fe-dependent R2s of an electron relay-competent residue at this position might reflect a selective advantage conferred by ensuring that the protein is stable to repeated activation events occurring in vivo. Adventitious reduction of $Y^{\bullet}$ in the conventional R2s is known to occur (*54*), and the corresponding reduction of the Mn^{IV} site in the active form of the class Ic proteins would produce the inactive Mn^{III}/Fe^{III} form. Reactivation of this form, either by reduction to Mn^{II}/Fe^{II} followed by reaction with O_2 or by direct reaction with H_2O_2 (*40*), would obviate the more costly de novo resynthesis of R2. The extra relay element may be conserved because it prevents deleterious side reactions that might otherwise lead to progressive inactivation during this redox cycling of the protein in vivo. The conservation of Y or W at this position could also reflect the existence of a specific accessory protein for delivering electrons in vivo. Recent studies on the *Ec* protein YfaE have suggested that it is just such a specific accessory factor, serving either to reduce the $Fe_2^{III/III}$ cluster in the inactive "met" ($Y^{\bullet}$-reduced) form of the protein to $Fe_2^{II/II}$ for subsequent reactivation by O_2, to deliver the extra electron during the activation reaction, or both (*55*). Y222 in *Ct* R2 seems ideally positioned to interact with a functionally homologous protein in *C. trachomatis* (Figure 1). Prospecting for genes that might encode such a factor is in progress.

Table 1: Comparison of the Intrinsic First-Order Rate Constants for Decay of the Mn^{IV}/Fe^{IV} Intermediate (k_{int}), the Second-Order Rate Constants for Its Reduction by Ascorbate (k_{asc}), and the Turnover Numbers (v/[R2 monomer]) of the wt *Ct* R2 Protein and Its Y222F, Y338F, and W51F Variants

R2 protein	k_{int} (s^{-1})	k_{asc} (mM^{-1} s^{-1})	v/[R2 monomer] (s^{-1})
wt	0.021	$(1.3 \pm 0.3) \times 10^{-1}$	0.60 ± 0.06
Y222F	0.002	$(2.0 \pm 0.5) \times 10^{-3}$	0.58 ± 0.02
Y338F	0.020	$(1.3 \pm 0.3) \times 10^{-1}$	<0.001
W51F	0.002	not determined	<0.001

SUPPORTING INFORMATION AVAILABLE

Comparison of the kinetics of the O_2 reaction of Mn^{II}/Fe^{II} Y222F *Ct* R2 obtained with the white light source and photodiode array detector to those obtained with the monochromatic light source and photomultiplier detector; time-dependent EPR spectra from the reactions of the wt, Y222F, and W51F R2 proteins with O_2; dependence of the kinetics of the Mn^{IV}/Fe^{IV} intermediate on the concentration of ascorbate in the reactions of the wt, Y338F, and Y222F proteins; Mössbauer spectra of the final products of the O_2 reactions of the wt, Y222F, Y338F, and W51F proteins recorded over a wide range of Doppler velocities; and figures validating the mass spectrometric activity assay. This material is available free of charge via the Internet at http://pubs.acs.org.

REFERENCES

1. Nordlund, P., and Reichard, P. (2006) Ribonucleotide reductases. *Annu. Rev. Biochem. 75*, 681–706.
2. Stubbe, J. (2003) Di-iron-tyrosyl radical ribonucleotide reductases. *Curr. Opin. Chem. Biol. 7*, 183–188.
3. Mao, S. S., Yu, G. X., Chalfoun, D., and Stubbe, J. (1992) Characterization of C439SR1, a mutant of *Escherichia coli* ribonucleotide diphosphate reductase: Evidence that C439 is a residue essential for nucleotide reduction and C439SR1 is a protein possessing novel thioredoxin-like activity. *Biochemistry 31*, 9752–9759.
4. Uhlin, U., and Eklund, H. (1994) Structure of ribonucleotide reductase protein R1. *Nature 370*, 533–539.
5. Stubbe, J., Nocera, D. G., Yee, C. S., and Chang, M. C. Y. (2003) Radical initiation in the class I ribonucleotide reductase: Long-range proton-coupled electron transfer? *Chem. Rev. 103*, 2167–2202.
6. Stubbe, J., and Ackles, D. (1980) On the mechanism of ribonucleoside diphosphate reductase from *Escherchia coli*. Evidence for 3′-C-H bond cleavage. *J. Biol. Chem. 255*, 8027–8030.
7. Stubbe, J., Ator, M., and Krenitsky, T. (1983) Mechanism of ribonucleoside diphosphate reductase from *Escherichia coli*. Evidence for 3′-C-H bond cleavage. *J. Biol. Chem. 258*, 1625–1631.

8. Licht, S., Gerfen, G. J., and Stubbe, J. (1996) Thiyl radicals in ribonucleotide reductases. *Science 271*, 477–481.
9. Stubbe, J., and Riggs-Gelasco, P. (1998) Harnessing free radicals: Formation and function of the tyrosyl radical in ribonucleotide reductase. *Trends Biochem. Sci. 23*, 438–443.
10. Ekberg, M., Pötsch, S., Sandin, E., Thunnissen, M., Nordlund, P., Sahlin, M., and Sjöberg, B.-M. (1998) Preserved catalytic activity in an engineered ribonucleotide reductase R2 protein with a nonphysiological radical transfer pathway. The importance of hydrogen bond connections between the participating residues. *J. Biol. Chem. 273*, 21003–21008.
11. Ekberg, M., Sahlin, M., Eriksson, M., and Sjöberg, B.-M. (1996) Two conserved tyrosine residues in protein R1 participate in an intermolecular electron transfer in ribonucleotide reductase. *J. Biol. Chem. 271*, 20655–20659.
12. Nordlund, P., Sjöberg, B.-M., and Eklund, H. (1990) Three-dimensional structure of the free radical protein of ribonucleotide reductase. *Nature 345*, 593–598.
13. Rova, U., Adrait, A., Pötsch, S., Gräslund, A., and Thelander, L. (1999) Evidence by mutagenesis that Tyr(370) of the mouse ribonucleotide reductase R2 protein is the connecting link in the intersubunit radical transfer pathway. *J. Biol. Chem. 274*, 23746–23751.
14. Rova, U., Goodtzova, K., Ingemarson, R., Behravan, G., Gräslund, A., and Thelander, L. (1995) Evidence by site-directed mutagenesis supports long-range electron transfer in mouse ribonucleotide reductase. *Biochemistry 34*, 4267–4275.
15. Seyedsayamdost, M. R., and Stubbe, J. (2006) Site-specific replacement of Y356 with 3,4-dihydroxyphenylalanine in the β2 subunit of *E. coli* ribonucleotide reductase. *J. Am. Chem. Soc. 128*, 2522–2523.
16. Seyedsayamdost, M. R., and Stubbe, J. (2007) Forward and reverse electron transfer with the Y_{356}DOPA-β2 heterodimer of *E. coli* ribonucleotide reductase. *J. Am. Chem. Soc. 129*, 2226–2227.
17. Seyedsayamdost, M. R., Xie, J., Chan, C. T. Y., Schultz, P. G., and Stubbe, J. (2007) Site-specific insertion of 3-aminotyrosine into subunit α2 of *E. coli* ribonucleotide reductase: Direct evidence for involvement of Y_{730} and Y_{731} in radical propagation. *J. Am. Chem. Soc. 129*, 15060–15071.
18. Atkin, C. L., Thelander, L., Reichard, P., and Lang, G. (1973) Iron and free radical in ribonucleotide reductase. Exchange of iron and Mössbauer spectroscopy of the protein B2 subunit of the *Escherichia coli* enzyme. *J. Biol. Chem. 248*, 7464–7472.
19. Bollinger, J. M., Jr., Edmondson, D. E., Huynh, B. H., Filley, J., Norton, J. R., and Stubbe, J. (1991) Mechanism of assembly of the tyrosyl radical-dinuclear iron cluster cofactor of ribonucleotide reductase. *Science 253*, 292–298.
20. Bollinger, J. M., Jr., Tong, W. H., Ravi, N., Huynh, B. H., Edmondson, D. E., and Stubbe, J. (1994) Mechanism of assembly of the tyrosyl radical-diiron(III) cofactor of *E. coli* ribonucleotide reductase. 2. Kinetics of the excess Fe^{2+} reaction by optical, EPR, and Mössbauer spectroscopies. *J. Am. Chem. Soc. 116*, 8015–8023.
21. Elgren, T. E., Lynch, J. B., Juarez-Garcia, C., Münck, E., Sjöberg, B.-M., and Que, L. (1991) Electron transfer associated with oxygen activation in the B2 protein of ribonucleotide reductase from *Escherichia coli*. *J. Biol. Chem. 266*, 19265–19268.
22. Ochiai, E., Mann, G. J., Gräslund, A., and Thelander, L. (1990) Tyrosyl free radical formation in the small subunit of mouse ribonucleotide reductase. *J. Biol. Chem. 265*, 15758–15761.
23. Baldwin, J., Krebs, C., Ley, B. A., Edmondson, D. E., Huynh, B. H., and Bollinger, J. M., Jr. (2000) Mechanism of rapid electron transfer during oxygen activation in the R2 subunit of *Escherichia coli* ribonucleotide reductase. 1. Evidence for a transient tryptophan radical. *J. Am. Chem. Soc. 122*, 12195–12206.
24. Bollinger, J. M., Jr., Tong, W. H., Ravi, N., Huynh, B. H., Edmondson, D. E., and Stubbe, J. (1994) Mechanism of assembly of the tyrosyl radical-diiron(III) cofactor of *E. coli* ribonucleotide reductase. 3. Kinetics of the limiting Fe^{2+} reaction by optical, EPR, and Mössbauer spectroscopies. *J. Am. Chem. Soc. 116*, 8024–8032.
25. Krebs, C., Chen, S., Baldwin, J., Ley, B. A., Patel, U., Edmondson, D. E., Huynh, B. H., and Bollinger, J. M., Jr. (2000) Mechanism of rapid electron transfer during oxygen activation in the R2 subunit of *Escherichia coli* ribonucleotide reductase. 2. Evidence for and consequences of blocked electron transfer in the W48F variant. *J. Am. Chem. Soc. 122*, 12207–12219.
26. Bollinger, J. M., Jr., Stubbe, J., Huynh, B. H., and Edmondson, D. E. (1991) Novel diferric radical intermediate responsible for tyrosyl radical formation in assembly of the cofactor of ribonucleotide reductase. *J. Am. Chem. Soc. 113*, 6289–6291.
27. Burdi, D., Sturgeon, B. E., Tong, W. H., Stubbe, J., and Hoffman, B. M. (1996) Rapid freeze-quench ENDOR of the radical **X** intermediate of *Escherichia coli* ribonucleotide reductase using $^{17}O_2$, $H_2{}^{17}O$, and ^2H_2O. *J. Am. Chem. Soc. 118*, 281–282.
28. Burdi, D., Willems, J.-P., Riggs-Gelasco, P., Antholine, W. E., Stubbe, J., and Hoffman, B. M. (1998) The core structure of **X** generated in the assembly of the diiron cluster of ribonucleotide reductase: $^{17}O_2$ and $H_2{}^{17}O$ ENDOR. *J. Am. Chem. Soc. 120*, 12910–12919.
29. Ravi, N., Bollinger, J. M., Jr., Huynh, B. H., Edmondson, D. E., and Stubbe, J. (1994) Mechanism of assembly of the tyrosyl radical-diiron(III) cofactor of *E. coli* ribonucleotide reductase. 1. Mössbauer characterization of the diferric radical precursor. *J. Am. Chem. Soc. 116*, 8007–8014.
30. Sturgeon, B. E., Burdi, D., Chen, S., Huynh, B. H., Edmondson, D. E., Stubbe, J., and Hoffman, B. M. (1996) Reconsideration of **X**, the diiron intermediate formed during cofactor assembly in *E. coli* ribonucleotide reductase. *J. Am. Chem. Soc. 118*, 7551–7557.
31. Willems, J.-P., Lee, H.-I., Burdi, D., Doan, P. E., Stubbe, J., and Hoffman, B. M. (1997) Identification of the protonated oxygenic ligands of ribonucleotide reductase intermediate **X** by Q-Band ^{1,2}H CW and pulsed ENDOR. *J. Am. Chem. Soc. 119*, 9816–9824.
32. Saleh, L., and Bollinger, J. M., Jr. (2006) Cation mediation of radical transfer between Trp48 and Tyr356 during O_2 activation by protein R2 of *Escherichia coli* ribonucleotide reductase: Relevance to R1-R2 radical transfer in nucleotide reduction? *Biochemistry 45*, 8823–8830.
33. Climent, I., Sjöberg, B.-M., and Huang, C. Y. (1992) Site-directed mutagenesis and deletion of the carboxyl terminus of *Escherichia coli* ribonucleotide reductase protein R2. Effects on catalytic activity and subunit interaction. *Biochemistry 31*, 4801–4807.
34. Jiang, W., Yun, D., Saleh, L., Barr, E. W., Xing, G., Hoffart, L. M., Maslak, M.-A., Krebs, C., and Bollinger, J. M., Jr. (2007) A manganese(IV)/iron(III) cofactor in *Chlamydia trachomatis* ribonucleotide reductase. *Science 316*, 1188–1191.
35. Jiang, W., Bollinger, J. M., Jr., and Krebs, C. (2007) The active form of *Chlamydia trachomatis* ribonucleotide reductase R2 protein contains a heterodinuclear Mn(IV)/Fe(III) cluster with $S = 1$ ground state. *J. Am. Chem. Soc. 129*, 7504–7505.
36. Voevodskaya, N., Lendzian, F., Ehrenberg, A., and Gräslund, A. (2007) High catalytic activity achieved with a mixed manganese-iron site in protein R2 of *Chlamydia* ribonucleotide reductase. *FEBS Lett. 581*, 3351–3355.
37. Roshick, C., Iliffe-Lee, E. R., and McClarty, G. (2000) Cloning and characterization of ribonucleotide reductase from *Chlamydia trachomatis*. *J. Biol. Chem. 275*, 38111–38119.
38. Jiang, W., Hoffart, L. M., Krebs, C., and Bollinger, J. M., Jr. (2007) A manganese(IV)/iron(IV) intermediate in assembly of the manganese(IV)/iron(III) cofactor of *Chlamydia trachomatis* ribonucleotide reductase. *Biochemistry 46*, 8709–8716.
39. Gill, S. C., and von Hippel, P. H. (1989) Calculation of protein extinction coefficients from amino acid sequence data. *Anal. Biochem. 182*, 319–326.
40. Jiang, W., Xie, J., Nørgaard, H., Bollinger, J. M., Jr., and Krebs, C. (2008) Rapid and quantitative activation of *Chlamydia trachomatis* ribonucleotide reductase by hydrogen peroxide. *Biochemistry 47*, 4477–4483.
41. Price, J. C., Barr, E. W., Tirupati, B., Bollinger, J. M., Jr., and Krebs, C. (2003) The first direct characterization of a high-valent iron intermediate in the reaction of an α-ketoglutarate-dependent dioxygenase: A high-spin Fe(IV) complex in taurine/α-ketoglutarate dioxygenase (TauD) from *Escherichia coli*. *Biochemistry 42*, 7497–7508.
42. Högbom, M., Stenmark, P., Voevodskaya, N., McClarty, G., Gräslund, A., and Nordlund, P. (2004) The radical site in Chlamydial ribonucleotide reductase defines a new R2 subclass. *Science 305*, 245–248.
43. Bollinger, J. M., Jr., Krebs, C., Vicol, A., Chen, S., Ley, B. A., Edmondson, D. E., and Huynh, B. H. (1998) Engineering the diiron site of *Escherichia coli* ribonucleotide reductase protein R2 to accumulate an intermediate similar to $\mathbf{H}_{peroxo}$, the putative peroxo-diiron(III) complex from the methane monooxygenase catalytic cycle. *J. Am. Chem. Soc. 120*, 1094–1095.
44. Moënne-Loccoz, P., Baldwin, J., Ley, B. A., Loehr, T. M., and Bollinger, J. M., Jr. (1998) O_2 activation by non-heme diiron proteins: Identification of a symmetric μ-1,2-peroxide in a mutant of ribonucleotide reductase. *Biochemistry 37*, 14659–14663.
45. Skulan, A. J., Brunold, T. C., Baldwin, J., Saleh, L., Bollinger, J. M., Jr., and Solomon, E. I. (2004) Nature of the peroxo

intermediate of the W48F/D84E ribonucleotide reductase variant: Implications for O_2 activation by binuclear non-heme iron enzymes. *J. Am. Chem. Soc. 126*, 8842–8855.
46. Baldwin, J., Voegtli, W. C., Khidekel, N., Moënne-Loccoz, P., Krebs, C., Pereira, A. S., Ley, B. A., Huynh, B. H., Loehr, T. M., Riggs-Gelasco, P. J., Rosenzweig, A. C., and Bollinger, J. M., Jr. (2001) Rational reprogramming of the R2 subunit of *Escherichia coli* ribonucleotide reductase into a self-hydroxylating monooxygenase. *J. Am. Chem. Soc. 123*, 7017–7030.
47. Valentine, A. M., Stahl, S. S., and Lippard, S. J. (1999) Mechanistic studies of the reaction of reduced methane monooxygenase hydroxylase with dioxygen and substrates. *J. Am. Chem. Soc. 121*, 3876–3887.
48. Yun, D., Krebs, C., Gupta, G. P., Iwig, D. F., Huynh, B. H., and Bollinger, J. M., Jr. (2002) Facile electron transfer during formation of cluster **X** and kinetic competence of **X** for tyrosyl radical production in protein R2 of ribonucleotide reductase from mouse. *Biochemistry 41*, 981–990.
49. Yun, D., Garcia-Serres, R., Chicalese, B. M., An, Y. H., Huynh, B. H., and Bollinger, J. M., Jr. (2007) (μ-1,2-Peroxo)diiron(III/III) complex as a precursor to the diiron(III/IV) intermediate **X** in the assembly of the iron-radical cofactor of ribonucleotide reductase from mouse. *Biochemistry 46*, 1925–1932.
50. Saleh, L., Krebs, C., Ley, B. A., Naik, S., Huynh, B. H., and Bollinger, J. M., Jr. (2004) Use of a chemical trigger for electron transfer to characterize a precursor to cluster **X** in assembly of the iron-radical cofactor of *Escherichia coli* ribonucleotide reductase. *Biochemistry 43*, 5953–5964.
51. Voevodskaya, N., Galander, M., Högbom, M., Stenmark, P., McClarty, G., Gräslund, A., and Lendzian, F. (2007) Structure of the high-valent $Fe^{III}Fe^{IV}$ state in ribonucleotide reductase (RNR) of *Chlamydia trachomatis*: Combined EPR, ^{57}Fe-, ^{1}H-ENDOR and X-ray studies. *Biochim. Biophys. Acta 1774*, 1254–1263.
52. Voevodskaya, N., Lendzian, F., and Gräslund, A. (2005) A stable Fe^{III}-Fe^{IV} replacement of tyrosyl radical in a class I ribonucleotide reductase. *Biochem. Biophys. Res. Commun. 330*, 1213–1216.
53. Voevodskaya, N., Narvaez, A. J., Domkin, V., Torrents, E., Thelander, L., and Gräslund, A. (2006) Chlamydial ribonucleotide reductase: Tyrosyl radical function in catalysis replaced by the Fe^{III}-Fe^{IV} cluster. *Proc. Natl. Acad. Sci. U.S.A. 103*, 9850–9854.
54. Hristova, D., Wu, C.-H., Jiang, W., Krebs, C., and Stubbe, J. (2008) Importance of the maintenance pathway in the regulation of the activity of *Escherichia coli* ribonucleotide reductase. *Biochemistry 47*, 3989–3999.
55. Wu, C. H., Jiang, W., Krebs, C., and Stubbe, J. (2007) YfaE, a ferredoxin involved in diferric-tyrosyl radical maintenance in *Escherichia coli* ribonucleotide reductase. *Biochemistry 46*, 11577–11588.

BI800881M